MCM-41 as a useful vector for rutin topical formulation: Synthesis, characterization and testing

(Article begins on next page)

08 July 2024

MCM-41 as a useful vector for rutin topical formulations: synthesis, characterization and testing

Gloria Berlier[a], Lucia Gastaldi[b], Simona Sapino[b], Ivana Miletto[a], Emanuela Bottinelli[a], Daniela Chirio[b], Elena Ugazio[b*]

[a]*Università di Torino, Dipartimento di Chimica and NIS, Nanostructured Interfaces and Surfaces Centre of Excellence, Via Giuria 7, 10125 Torino, Italy.*

[b]*Università di Torino, Dipartimento di Scienza e Tecnologia del Farmaco, Via Giuria 9, 10125 Torino, Italy.*

*Corresponding author. Tel: +39 0116707192; Fax: +39 0116707687

E-mail address: elena.ugazio@unito.it

Abstract

Rutin, the glycoside of quercetin, could be used in topical preparations because of its antioxidant and radical scavenging properties, but its employ in cosmetic and pharmaceutical products is limited by poor physico-chemical stability. These issues were addressed by preparing, characterizing and testing rutin inclusion complexes with MCM-41 mesoporous silica. The effect of surface functionalization with aminopropyl groups (NH_2-MCM-41) on the molecules properties was studied. The organic/inorganic interaction was confirmed by XRD, TGA, gas-volumetric analysis (BET) and FTIR spectroscopy. In particular, the high inclusion of rutin in the pores of NH_2-MCM-41 was confirmed by

many techniques, while FTIR allowed to analyze with great detail the molecular interaction with the inorganic and hybrid surface. Rutin was stabilized against UV degradation, mostly by its inclusion in NH$_2$-MCM-41. *Ex vivo* studies showed a greater accumulation in porcine skin in the case of rutin complexed with NH$_2$-MCM-41. Not only antioxidant properties of rutin were maintained after immobilization but, with aminopropyl silica, the metal-chelating activity increased noticeably. The immobilization of rutin in aminopropyl silica resulted in better performance in terms of activity and photostability, suggesting the importance of functionalization in stabilizing organic molecules within silica pores.

Keywords: Mesoporous silica nanoparticles, Flavonoids, Photostability, Skin permeation, Antiradical activity

1. Introduction

Rutin (quercetin-3-O-rutinoside, Scheme 1), the glycoside of quercetin, is abundantly found and distributed in higher plants such as in buckwheat seed, fruits and fruit rinds, especially citrus fruits (orange, grapefruit, lemon, and lime). Rutin has significant scavenging properties that act on reactive oxygen species (ROS) such as hydroxyl, superoxide, and peroxyl radicals. Due to the presence of many phenolic hydroxyl groups typical of flavonoids, rutin can donate hydrogen atoms to radicals, thus acting as radical chain terminator. Newly formed flavonoid radicals are delocalized on the whole molecule, making them far less aggressive (Dall'Acqua et al., 2012).

These peculiarities have been shown in many *in vitro* experiments (Graefe et al., 2001, Middleton et al., 2000). Its multiple pharmacological activities include antiinflammatory (Rabiskova et al., 2012)

3

and vasoactive, antitumour and antiviral properties (Mauludin et al., 2009). Rutin is also known to have preventing properties being a hypolipidaemic and cardioprotective agent (Karthick and Prince, 2006). This flavonoid has a high absorption with a maximum in the UVA (λ_{max} 355 nm) and one in the UVC (λ_{max} 257 nm). The mechanism of rutin photoprotection consists in UV radiation absorption resulting in prevention of ROS formation and the ensuing DNA damage. The absorbed UV energy is dissipated as heat, light, or through the decomposition of rutin itself which takes place in a mixture of three products obtained by opening the C ring. Unfortunately, the potential topical usefulness of this natural compound is limited by its lability, photodegradation being observed in creams (Scalia, 2009).

The potential of rutin for topical applications, coupled to the physico-chemical drawbacks, motivates the search for an efficient vector for its stabilization in pharmaceutical formulations. To this aim, MCM-41 mesoporous silica was selected, following the promising results obtained with other antioxidant molecules, including quercetin (Berlier et al., 2013, Gastaldi et al., 2012).

The employ of ordered mesoporous materials as drug delivery systems (DDS) was firstly reported by Vallet-Regí et al. in 2001. Since then, the reports about the use of mesoporous silica (or bioactive oxides) as DDS have increased exponentially (Ambrogio et al., 2011, Ferris et al., 2009, Fontecave et al., 2012, Li et al., 2012, Manzano et al., 2009, Rosenholm et al., 2012, Vivero-Escoto et al., 2010, Wang, 2009), so that they are now addressed as "multifunctional platforms", able to deliver therapeutic/diagnostic agents (Meng et al., 2012). Moreover, MCM-41 positive effects on photostability of drugs and sunscreens have been already reported in the literature (Ambrogi et al., 2012, Ambrogi et al., 2013). The reasons for this success are easily understood: extremely high surface area, ordered porosity and large pore volume are ideal properties for high drug loading and a diffusion-driven gradual release (Andersson et al., 2004, Cauda et al., 2009, Vallet-Regí et al., 2007). Silica is expected to have relatively good stability and biocompatibility, even if its fate in physiological fluids and the actual effect on cells is still the object of many studies, especially when nanoparticles are

4

employed (Di Pasqua et al., 2008, Fontecave et al., 2012, Garcia et al., 2009, Huang et al., 2010, Lin et al., 2011, Lu et al., 2010, Mortera et al., 2010, Tao et al., 2008, Trewyn et al., 2008).

Importantly, the Si-OH rich silica surface can be easily functionalized to optimize the interaction with the drug (Manzano et al., 2009, Rosenholm and Linden, 2008) to covalently link agents for targeted delivery (Ferris et al., 2011, Lu et al., 2012, Mamaeva et al., 2011, Rosenholm et al., 2009), to modify surface charge and properties affecting the interactions with biomolecules (Izquierdo-Barba et al., 2011, Liong et al., 2009) or improving permeability through cellular membranes (Meng et al., 2011a, Meng et al., 2011b).

In this work MCM-41 was employed to prepare inclusion complexes with rutin and its properties were compared to those obtained with an aminopropyl functionalized analogue. The results include the sample preparation and physico-chemical characterization, with particular attention to the interaction of rutin with the silica surface, studied by infrared spectroscopy. The drug diffusion through a cellulose membrane was followed, and the properties of the included molecule (photostability, antioxidant and chelating activities) were analyzed. These tests were performed in media of growing complexity: a hydroalcoholic solution and an O/W emulsion, both at pH 5.0, with a view to the potential application of the developed complexes for topical applications. Accordingly, transepidermal permeation and skin uptake were monitored by employing porcine skin, an efficient model due to morphological and functional similarity to human one (epidermal thickness and lipid composition). The comparison among the performances of the two complexes and free rutin are discussed in relation to the studied physico-chemical properties.

2. Materials and methods

2.1. Materials

5

Acetone, absolute ethanol, methanol and trisodium citrate dihydrate were purchased from Carlo Erba (Milan, Italy). Acetic acid, ferrozine (3-(2-pyridyl)-5,6-diphenyl-1,2,4-triazine-4',4''-disulfonic acid sodium salt), iron(II)sulfate and rutin trihydrate (R) were purchased from Fluka (Milan, Italy). Anhydrous citric acid, dimethicone (Abil 350), glycerin, imidazolidinyl urea (Kemipur 100), isononyl isononanoate (Tegosoft CI) were products ACEF (Fiorenzuola D'Arda, Piacenza, Italy). Carbomer (Carbopol ETD 2001) was from Noveon (Brussels, Belgium). TiO_2 (Aeroxide P 25) was a Degussa product (Milan, Italy). DPPH$^\bullet$ (2,2-diphenyl-1-picrylhydrazyl free radical), n-cetyltrimethylammonium bromide (CTAB), silica ($SiO2$), 3- aminopropyl triethoxysilane (APTES), toluene and sodium azide were purchased from Sigma-Aldrich (St. Louis, MO, USA). Potassium palmitoyl hydrolyzed wheat protein/glyceryl stearate/cetearyl alcohol (Phytocream 2000) was a Sinerga product (Pero, Italy). Esters of 4-hydroxybenzoic acid in 2-phenoxyethanol (Uniphen P-23) were from Induchem (Volketswil, Zürich, Switzerland).

2.2. Synthesis

Purely siliceous mesoporous MCM-41 was synthesized according to the literature, employing CTAB as the Structure Directing Agent (SDA) and fumed silica (Beck et al., 1992) SDA was removed by calcination at 550 °C, first under nitrogen and subsequently under oxygen flow.

NH_2-MCM-41 was prepared by suspending 1 g of calcined MCM-41 in 30 mL of toluene. Next, 0.6 mL of APTES were added drop-wise and the mixture was allowed to reflux for 8 h. The reaction solution was centrifuged and the deposited gel washed first with ethanol and then with deionized water. The obtained white solid was filtered, washed with methanol and dried *in vacuum* (Parida and Rath, 2009).

R inclusion complexes were prepared by impregnation method in 1/1 w/w ratio. 200 mg of silica (MCM-41 or NH_2-MCM-41) were outgassed at 150 °C for 1 h to remove the adsorbed water and were

then added to 5.0 mL of saturated R methanol solution (40 mg/mL). The mixtures were kept under magnetic stirring at room temperature (RT) for 24 h and after centrifugation each precipitate was dried under *vacuum*. The resulting complexes are hereafter labeled as R/MCM-41 and R/NH$_2$-MCM-41.

2.3. Sample preparation and analysis

The aqueous system was obtained by magnetically mixing ethanol and acetate buffer in 15/85 v/v ratio such to have a final pH of 5.0. An amount of R, free or immobilized, was finally dispersed into the mixture such to achieve the desired concentration (0.25 or 0.5 mM). The O/W emulsion was prepared gradually dispersing by a T25 Basic Ultra-Turrax homogenizer (IKA, Staufen, Germany) the melted lipid phase (2.5 g Phytocream 2000, 6.5 g Tegosoft CI and 1.0 g Abil 350) in the aqueous one (0.1 g Carbopol ETD 2001, 4.5 g glycerin and 65.4 g ultrapure water) previously heated at about 75 °C. A weighted amount of R, R/MCM-41 or R/NH$_2$-MCM-41, previously dispersed in 20 mL of water, was added by homogenization to obtain 1.0 mM final flavonoid concentration. If necessary the pH was adjusted to 5.0 with 0.5 N HCl.

UV-Vis analysis was performed both in methanol and in ethanol/acetate buffer (15/85 v/v) mixture (pH 5.0) by using a DU 730 UV/Vis scanning spectrophotometer (Beckman Coulter, Brea, CA, USA). The calibration curve was determined over the range 0.20-5.50×10^{-5} M. The resulting molar extinction coefficients (ε) were 15741 M^{-1} (R^2 = 0.999) and 18694 M^{-1} (R^2 = 0.999), respectively. Each quantified datum was averaged from triplicate analysis.

For HPLC analysis a system consisting of a LC-10AD pump unit control and a C-R3A chromatopac integrator (Shimadzu, Kyoto, Japan), an UV-1575 detector (Jasco, Oklahoma City, OK, USA), and a RP-C18 column (150×4.6 mm; 5 μm) was employed. The mobile phase was a mixture of methanol/water/acetic acid (45/52/3 v/v/v) with flow rate of 0.8 mL/min. The elution profile was monitored at 355 nm and the retention time of R was around 4.0 min. HPLC standard curve was

7

generated by plotting the peak area values *vs* pure R concentrations over the range $0.50\text{-}7.50\times10^{-5}$ M in ethanol/acetate buffer (15/85 v/v) mixture (pH 5.0) (y = 3.0×1010 x - 57129, R^2=0.996) and over the range $0.05\text{-}1.00\times10^{-4}$ M in methanol (y = 1.0×1010x - 28078, R^2=0.999). Each quantified datum was averaged from triplicate analysis.

The spectrophotometric evaluation of R loaded into the complexes was carried out by dispersing 2.0 mg of R/MCM-41 or R/NH$_2$-MCM-41 into absolute methanol (5.0 mL) with stirring at RT in darkness for 4 h. The loading content (% R) was calculated according to the following equation:

$$\% \text{ R} = (\text{amount of R in the complex/total amount of the complex}) \times 100.$$

2.4. Physico-chemical characterization

Powder X Ray Diffraction (XRD) patterns were collected on a X'Pert Pro Bragg Brentano diffractometer (Philips, Milan, Italy) using Cu Kα radiation (40 mA and 45 kV), with a scan speed of $0.01°$ min^{-1}.

Thermogravimetric analysis (TGA) was carried out on a Q600 thermogravimetric analyzer (TA Instruments, Lukens, DE, USA) heating the samples at a rate of 10 °C from RT to 1000 °C in a nitrogen flow. Before starting measurements, samples were equilibrated at 30 °C. Once reached the final temperature an isotherm was run for 15 min in air.

Gas-volumetric analysis (N$_2$ adsorption–desorption isotherms at liquid nitrogen temperature, LNT) was employed to measure specific surface area (SSA), pore volume and size with an ASAP 2020 physisorption analyzer (Micromeritics, Norcross, GA, USA). SSA and average pore size were calculated by the Brunauer–Emmet–Teller (BET) and the Barrett–Joyner–Halenda (BJH) methods, respectively. For the latter the Kruk-Jaroniec-Sayari (KJS) equations were employed in the adsorption isotherms. Volume of the meso- and macropores (interparticle porosity) was calculated on the

adsorption branch with the BJH/KJS model in the 25-50 and 200-1000 Å ranges, respectively. Prior to analyses, the samples were outgassed overnight at RT.

Fourier transform infrared spectra (FTIR) were recorded with a IFS 88 spectrometer (Bruker Corporation, Billerica MA, USA) with a DTGS detector, working with resolution of 4 cm^{-1} over 64 scans. Samples were in the form of self-supporting pellets suitable for transmission infrared experiments and were placed in a quartz cell equipped with KBr windows, designed for *in vacuum* RT studies. Before FTIR analysis the samples were outgassed at RT to remove physically adsorbed water and impurities. Spectra of pure R were obtained in KBr pellets.

2.5. *Testing of complex properties*

2.5.1. *UV-irradiation test*

The photostability study was performed in two different media: the ethanol/acetate buffer (15/85 v/v) mixture and the O/W emulsion described above, both added with a well known photocatalyst, TiO_2. Particularly, 0.05 mM R, free or immobilized, and 0.05% w/v TiO_2 were added to the ethanol/acetate buffer mixture, while 1.00 mM and 1.0% w/w, respectively, were employed in the O/W emulsion.

All the samples (10.0 mL) were placed under stirring at 10.0 cm from a UVB lamp with 2.5×10^{-4} W cm^{-2} power irradiance. At scheduled time until 180 min, 200 μL were withdrawn and properly diluted with methanol for HPLC analysis. Photodegradation kinetics were studied by plotting the percentage of non degraded R as a function of irradiation time. The percentage of non degraded R was calculated as follows:

$$\% \text{ non degraded R} = C_t/C_0 \times 100$$

where C_0 is the R concentration at zero time while C_t is the R concentration after a given irradiation time (*t*). The study was carried out in triplicate.

2.5.2. In vitro diffusion studies

A device consisting of two horizontal glass cells (volume 22.0 mL, donor area 3.3 cm^2), separated by a Spectra/Por cellulose dialysis membrane (12000-14000 MWCO Spectrum Labs), was employed. The ethanol/acetate buffer mixture was chosen both as donor and receiving phase. In the former, R (free or immobilized) was dispersed to get 0.25 mM final concentration. The apparatus, sheltered from light, was maintained under stirring for 4 h. Aliquots (200 µL) of the receiving phase were withdrawn at scheduled time for HPLC analysis.

2.5.3. Ex vivo experiments

Transepidermal permeation and skin uptake were determined using vertical Franz cells and porcine skin. Skin slices were isolated with a dermatome from outer side of pig ears freshly obtained from a local slaughterhouse and then stored for at least 24 h at -18 °C. Prior to each experiment, the excised skin was rinsed with normal saline solution and pre-hydrated by floating it in 0.002% (w/v) sodium azide aqueous solution. The skin was then sandwiched between the two cells with the *stratum corneum* side upwards. The receptor chamber was filled with 6 mL of normal saline solution/ethanol (85/15 v/v) mixture.

The test formulations (500 µL), consisting of free or immobilized R, dispersed into ethanol/acetate buffer mixture (0.25 mM) or in O/W emulsion (1.0 mM), were applied to the skin surface (available diffusion area of 1.60 cm^2). The content of the receptor chamber, continuously stirred at 37 °C, was removed at appropriate intervals (1, 2, 3, 4, 5, 6, 24 h) for R determination and the cell was immediately refilled with fresh receptor solution. After 24 h, the application site of the skin was washed with normal saline solution to remove excess R on the surface. The skin was then cut with scalpel into small pieces and added with methanol (2.0 mL) for R extraction. After 4 h of magnetic stirring at RT, the resulting suspension was centrifuged and the supernatant was assayed by HPLC

analysis. The skin uptake was expressed as μg R/cm^2 skin diffusion area.

2.5.4. Antiradical and metal chelating activities

The antioxidant activity was determined based on the ability of the antioxidants to act as radical scavengers towards the stable DPPH•, with slight modifications of a literature method (Gulcin, 2006). Briefly, dilutions (100.0 μL) of R, free or immobilized, in the range 5.0-100.0 μM were added to 5.0 mL of DPPH˙ saturated ethanol/water (50/50 v/v) solution. Samples were kept under magnetic stirring for 10 min at RT in darkness to reach the steady-state condition; after sample centrifuging, absorbance readings were taken at 515 nm. The percentage of radical scavenging activity (% RSA) was determined through the following equation:

$$\% \text{ RSA} = [(A_0 - A_x)/A_0] \times 100$$

where A_0 is the absorbance of the control and A_x is the absorbance in the presence of antioxidant. The percentage of RSA was plotted against each R dilution.

The ability of R, R/MCM-41 or R/NH2-MCM-41 to chelate ferrous ion (Fe^{2+}) was investigated based on the method employed by Dinis *et al*. (Dinis et al., 1994). In this slightly modified assay, different concentrations of antioxidant (5-50.0 μM) in 4.0 mL ethanol/water solution (15/85 v/v, pH 5.0) were incubated with $FeSO_4$ (0.05 mL, 2.0 mM) and ferrozine aqueous solution (0.20 mL, 2.0 mM). After the mixtures had reached equilibrium (10 min of magnetic stirring, RT), they were centrifuged and then spectrophotometrically analyzed at 562 nm. The ability of each antioxidant sample to inhibit the formation of the ferrous-ferrozine complex, expressed as its Fe^{2+} chelating effect (% chelating activity), was then calculated using the equation:

$$\% \text{ chelating activity} = [(A_0 - A_x)/A_0] \times 100$$

where A_0 is the absorbance of a solution containing only $FeSO_4$ and ferrozine, while A_x is the absorption of the sample containing the flavonoid.

3. Results and discussion

3.1. Physico-chemical characterization

3.1.1. General properties of R/silica complexes

The general properties of the R/silica complexes were characterized by XRD, TGA and gas-volumetric analyses.

Low angle XRD patterns of the prepared R/MCM-41 and R/NH$_2$-MCM-41 samples are reported in Fig. 1, together with the diffraction patterns of the corresponding matrices. The samples display the typical (100), (110), (200) and (210) peaks related to a hexagonal network of mesopores (P6mm), with the latter ones suggesting the presence of a long range order. The intensity of the peaks decreases in the order MCM-41 > NH$_2$-MCM-41 > R/MCM-41 and are almost nonexistent in R/NH$_2$-MCM-41. This could be taken as an indication of the effective inclusion of both aminopropyl functional groups and R molecules within the silica pores. Noticeably, R inclusion affects the peak intensity to a more considerable extent with respect to surface functionalization with aminopropyl groups, in agreement with the relatively large molecular size (Scheme 1). We underline the fact that no diffraction peaks related to rutin were observed in all samples, thus excluding the presence of small rutin crystalline aggregates on the external surface of mesoporous silica.

TGA was employed to get information on the interaction of R molecules with the surface of the inorganic matrix and to measure the drug loading, which was compared to the values calculated by spectrophotometric analysis (Table 1).

The thermograms of the two complexes are compared to those obtained on the parent matrices in Fig. 2. All measurements were performed in nitrogen flow, while an isotherm in air was carried out at the end of the ramp, in order to burn out the carbonaceous residues from pyrolysis processes and measure the total organic weight loss. This is the reason for the vertical weight loss at 1000 °C observed in Fig. 2.

12

Table 1. Data from thermogravimetric analysis (percentage weight loss) and from UV-Vis spectrophotometric analysis (percentage of loading).

Samples	TGA				UV-Vis
	Water [a]	Hydroxyl groups	Aminopropyl groups	Rutin	% R (w/w)
MCM-41	3.4	7.3	-	-	-
NH$_2$-MCM-41	2.8	1.7 [b]	13.6	-	-
R/MCM-41	1.2	6.2 [b]	-	12.8	13.1
R/NH$_2$-MCM-41	3.2	3.1 [b]	13.6	18.1	18.1

[a]Measured in the 30-100 °C range. [b]Measured in the 700-1000 °C range, before isotherm in air.

The same experiment performed on pure R resulted in three weight losses: a first one around 100 °C corresponding to hydration water molecules, a main weight loss at 267 °C and a more gradual one around 440 °C, which were ascribed to the degradation of the disaccharide (rutinose) and of the aglycone (quercetin), respectively (data not reported for sake of brevity).

MCM-41 thermogram (full black line in Fig. 2) is characterized by a first weight loss around 100 °C related to adsorbed water, and by a gradual decrease in the whole temperature range related to the process of surface dehydroxylation (hydrolysis of Si-OH bonds to form water and Si-O-Si bridges). In addition to water loss, NH$_2$-MCM-41 shows a main weight loss around 540 °C ascribed to the decomposition of the aminopropyl chains. The amount of covalently linked organic chains was estimated by subtracting to the whole weight loss (excluding physisorbed water) the weight loss

between 700 and 1000 °C, assuming that it is due to hydrolysis of unreacted Si-OH groups (Table 1).

In both R/MCM-41 and R/NH$_2$-MCM-41 complexes additional weight losses are observed around 260 and 440 °C, which are easily assigned to the thermal decomposition of adsorbed R. Noticeably, the degradation phenomena occur at the same temperature of pure R, suggesting that the inclusion in silica pores did not affect its thermal stability.

R loading was calculated by subtracting to the total weight loss of the two complexes those related to adsorbed water, dehydroxylation and, in the case of R/NH$_2$-MCM-41, to the aminopropyl moieties. The resulting values are consistent with the loading calculated by spectrophotometric analysis after extraction with absolute methanol (last column in Table 1). These values were checked by measuring R amount remained in the supernatant after the impregnation procedure (not reported).

It can be clearly seen that the storage capacity improved passing from bare MCM-41 to NH$_2$-MCM-41, demonstrating the significant contribution of the aminopropyl functionalization to drug uptake.

The results of gas-volumetric analysis of the two complexes are reported together with those obtained on the parent matrices for comparison. Most samples show the type IV isotherm typical of mesoporous materials: the slope at intermediate p/p^0 (below 0.4) is related to the capillary condensation of nitrogen inside the mesopores, while the type H1 hysteresis loop at high p/p^0 (<0.90) is due to interparticle macroporosity (Fig. 3). When comparing R/MCM-41 with the parent silica, a consistent decrease in SSA and pore volume is observed, both in the meso- and macropores range (Table 2), suggesting the presence of R both inside the mesopores and in the interparticle porosity. The average pore diameter, on the contrary, is not sensibly affected by inclusion. This could indicate a non uniform distribution of R within the silica pores.

The nitrogen isotherm of NH$_2$-MCM-41 clearly shows a decrease of SSA and pore diameter with respect to bare MCM-41, confirming the success of surface functionalization. This is testified by a shift to lower p/p^0 of the isotherm slope related to mesopores, corresponding to a change in pore diameter

from 39 to 33 Å (Fig. 4 and Table 2). In this case impregnation with R has a dramatic effect on all parameters, so that the corresponding values listed in Table 2 are only indicative, being below the sensitivity limit of the instrument. This result, in agreement with XRD data and with the high loading measured by TGA and spectrophotometric measurements, suggests an effective inclusion of R within silica porosity.

Table 2. Textural properties of the silica-based samples

Samples	Mesopore diameter (Å)	SSA ($m^2 \cdot g^{-1}$)	Mesopore volume ($cm^3 \cdot g^{-1}$)	Macropore volume ($cm^3 \cdot g^{-1}$)
MCM-41	39	1133	0.68	0.87
NH_2-MCM-41	33	709	0.47	0.48
R/MCM-41	39	601	0.40	0.45
R/NH_2-MCM-41	-	~71	~0.27	~0.034

3.1.2. Study of R interaction with the silica surface

The interaction of R molecules with the bare and functionalized silica surface was studied by employing infrared spectroscopy. For sake of clarity, the infrared spectra of R/MCM-41 and R/NH_2-MCM-41 samples will be discussed separately, by comparing them with the spectra of R (dispersed in KBr) and of the parent silica. R is a complex molecule, displaying the flavonoid structure of quercetin linked to a rutinoside unit in the 3 position (Scheme 1). This implies that, with respect to quercetin,

15

more hydroxyl groups are available for interaction with the hydrophilic silica surface.

In the high frequency range (top panel of Fig. 5) the infrared spectrum of R is characterized by a broad and structured adsorption between 3700 and 2700 cm^{-1} (maxima at 3430 and 3367 cm^{-1}), which is easily assigned to inter and intra-molecular hydrogen bonding involving both the quercetin aglycone and the rutinoside disaccharide. Weak bands are observed between 3000 and 2850 cm^{-1}, related to the antisymmetric and symmetric stretching modes (ν_{as} and ν_s) of -CH$_3$ and -CH$_2$- groups of the disaccharide. Similarly to what observed for quercetin (Berlier et al., 2013), the νCH modes of the aglycone are too weak to be observed.

The low energy range is richer in information, showing many well resolved peaks (bottom panel of Fig. 5). Only the region between 1750 and 1300 cm^{-1} is reported, since in the MCM-41 complexes the lower region is dominated by the intense modes of silica. Based on their position the observed bands can be assigned to the carbonyl group (νC=O at 1654 cm^{-1}), the aromatic ring vibrations (νC=C at 1606, 1566 and 1502 cm^{-1}) and the –CH$_3$ bending mode (δCH$_3$ at 1358 cm^{-1}). The spectral region between 1475 and 1400 cm^{-1} is more complex, since there could be superimpositions of δCH and δCH$_2$ modes with the δOH/νC–O combination modes of the alcoholic/phenolic groups.(Socrates, 2006) A more detailed assignment will be put forward in the following, on the basis of the changes induced by R adsorption on the silica surface.

Coming to the R/MCM-41 complex, in the high energy region the spectrum is dominated by a very intense absorption between 3780 and 2750 cm^{-1}, due to the occurring of hydrogen bonding interactions of R with surface Si-OH groups. This is confirmed by comparison with the spectrum of bare MCM-41: in the complex the intensity of the sharp band at 3742 cm^{-1} related to isolated Si-OH is halved, with a corresponding increase in the intensity and width of the absorption at lower energy. The νCH bands of R are superimposed to the tail of this band. The non perfect correspondence in this region may be

ascribed to the presence of hydrocarbon impurities adsorbed on the silica surface.

The low energy range spectrum of R/MCM-41 is almost coincident with that of free R, confirming the structural integrity of the molecule (bottom panel in Fig. 5). Noticeably, the νC=O band at 1654 cm^{-1} is practically unaffected by the interaction with the silica surface, as happens to almost all νC=C aromatic and to the δCH$_3$ band at 1358 cm^{-1}. This represents a difference with respect to what observed for quercetin (Berlier et al., 2013), and could be explained by assuming that the surface interaction is modulated by the presence of the rutinoside disaccharide, thanks to its most hydrophilic nature and/or because of steric hindrance. The main differences regard the aromatic νC=C component at 1566 cm^{-1} and, more importantly, the band at 1457 cm^{-1}, which decreases in intensity and is red-shifted. On these basis, we hypothesize that the latter is mainly due to the δOH/νC–O of the rutinoside moiety.

The spectra obtained on R/NH$_2$-MCM-41, together with those of NH$_2$-MCM-41 are showed in Fig. 6. The spectrum of NH$_2$-MCM-41 shows the features expected for a functionalized surface. In the high energy region (top panel of Fig. 6) the almost complete consumption of isolated Si-OH groups can be seen, with a residual weak band at 3730 cm^{-1}, related to Si-OH groups involved in hydrogen bonding as acceptors (Braschi et al., 2012, Tosoni et al., 2008). Clear bands at 3364 and 3298 cm^{-1} (NH$_2$ ν_{as} and ν_s, respectively) and at 2936 and 2867 cm^{-1} (CH$_2$ ν_{as} and ν_s) confirm the presence of the aminopropyl chains. In the same region the R/NH$_2$-MCM-41 complex is characterized by an increase of the broad band

due to hydrogen bonding, and by relatively intense bands in the νCH region. The latter can be interpreted as the summing up of bands due to the aminopropyl chains with those of R molecules. As for hydrogen bonding, we propose that it is involving R molecules with residual Si-OH groups, as testified by the disappearance of the weak band at 3730 cm^{-1}. The low energy region of NH$_2$-MCM-41 (bottom panel of Fig. 6) shows, superimposed to the weak overtone and combination modes of silica,

17

the vibrational modes of the aminopropyl chains (δNH_2 at 1594 cm^{-1} and δCH_2 between 1500 and 1400 cm^{-1}). Also in this case the bands related to R are observed, confirming the preservation of the molecular structure. However, we underline a more evident perturbation of the R vibrational modes with respect to what observed on R/MCM-41. More in detail, the $\nu C=O$ band at 1654 cm^{-1} is slightly red-shifted, two of the aromatic $\nu C=C$ modes increase in intensity and change their positions (1566 and 1502 cm^{-1}), as happens to the band at 1457 cm^{-1} previously assigned to the of $\delta OH/\nu C-O$ combination mode of the disaccharide.

An explanation at the molecular level of the above described transformations upon R inclusion within the pores of NH$_2$-MCM-41 is obviously impossible without employing theoretical calculations. However, the observed changes clearly indicate a different perturbation of R functional groups when aminopropyl groups are anchored on the silica surface. The red-shift of the carbonyl bands and the evident perturbation of the aromatic absorptions resemble the situation observed in the case of quercetin, where a hydrogen bonding of isolated molecules with silica surface was proposed (Berlier et al., 2013). On this basis, we can put forward the hypothesis that, while on R/MCM-41 the interaction of R with surface Si-OH takes place mainly through the rutinoside disaccharide (probably as a consequence of hydrophilic affinity and steric hindrance), when the surface of silica is functionalized with aminopropyl chains these take an important role in the Van der Waals interactions with the quercetin aglycone.

3.2. Testing of complex properties

3.2.1. Photodegradation study

In this study the effect of mesoporous silica, bare or amino-functionalized, was considered in the attempt to protect R from photodegradation.

UV detection of R by HPLC reveals a peak at 355 nm that under UVB light decreases. In this

experiment R, free or complexed, was dispersed in two different media employing TiO_2 as a photocatalyst. Firstly, a hydroalcoholic solution with 0.05% w/v TiO_2 was chosen for a preliminary screening, secondly an O/W emulsion containing a higher TiO_2 percentage (1.0% w/w) was selected as more representative of commercial suncare products.

The percentages of non degraded R after both 90 and 180 min of illumination were reported in Table 3; the corresponding photodegradation rate equations were also calculated (Table 4).

Table 3. Percentages of non-degraded R, free or immobilized, in ethanol/acetate buffer (15/85 v/v, pH 5.0) and in O/W emulsion (pH 5.0), after 90 and 180 min of UVB irradiation

	% non-degraded R			
Samples	Solution		O/W emulsion	
	90 min	*180 min*	*90 min*	*180 min*
R	74.4 (± 3.2) %	45.8 (± 2.2) %	87.8 (± 2.5) %	70.1 (± 4.2) %
R/MCM-41	62.6 (± 2.9) %	33.9 (± 5.4) %	89.9 (± 1.3) %	81.9 (± 2.6) %
R/NH$_2$-MCM-41	98.8 (± 1.2) %	66.3 (± 3.7) %	97.0 (± 4.5) %	81.5 (± 2.2) %

Table 4. Photodegradation equations of R, free or immobilized, in ethanol/acetate buffer (15/85 v/v, pH 5.0) and in O/W emulsion (pH 5.0), upon UVB irradiation (180 min)

Samples	Solution		O/W emulsion	
R	y = -0.302 x + 100	R^2= 0.992	y = -0.150 x + 100	R^2= 0.959
R/MCM-41	y = -0.393 x + 100	R^2= 0.989	y = -0.110 x + 100	R^2= 0.942
R/NH$_2$-MCM-41	*		y = -0.107 x + 100	R^2= 0.945

* Data cannot be linearized

In the first dispersion system, R in aminopropyl silica is completely stable for 90 min whereas R in bare MCM-41 is less photostable than free R. In O/W emulsion the results highlighted that R incorporation into both mesoporous silica improves its photostability and also in this case R/NH$_2$-MCM-41 is completely stable for 90 min. Equations show pseudo-zero order kinetics in all the cases (except for R/NH$_2$-MCM-41) with rates lower in O/W emulsion than in hydroalcoholic solution.

Summarizing, the above findings confirm those obtained with complex characterization; NH$_2$-MCM-41 can perform a best protective effect against UVB because it establishes stronger bonds with the flavonoid. For this reason aminopropyl-functionalized silica, especially in O/W emulsion, can be proposed as a valid excipient for antioxidant photostability enhancement that is of paramount importance because drug photostability improvement can be useful to increase drug efficacy, safety and shelf-life.

3.2.2. Permeation studies

Based on the above results, a study of permeation from a hydroalcoholic mixture through a dialysis membrane. These experiments also allowed to estimate the kinetics of R release from the silica vehicles. After 4 h diffusion, the cumulative profiles followed a pseudo-zero order kinetics both for

pure R and for the complexes. As expected, the diffusion from the complexes was delayed compared with that of free R, testifying a certain organic/inorganic interaction. The complexes demonstrated similar trends, with the lower diffusion rate observed for R/NH$_2$-MCM-41 (Fig. 7). In any case the flavonoid was released along time; it could be hypothesized that when it was dispersed in ethanol/acetate buffer mixture a competition between silica and dispersion medium occurred so that R was released from silica. Moreover it is evident that no covalent bonds were involved in the complex formation also in the case of R/NH$_2$-MCM-41.

An *ex-vivo* permeation study was performed to evaluate the possible employment of mesoporous silica matrices as vehicles for dermal delivery and, more specifically, to develop an effective R based formulation for the prevention of free radical-induced skin damage.

Using ethanol/acetate buffer mixture as donor phase, all studied samples showed a negligible permeation until 6 h; after 24 h the amount of permeated R is very small for all systems, besides complexes showed smaller permeation than free R confirming the interaction between the flavonoid and the inorganic matrix that retains R and prevents the permeation (Fig. 8). Also accumulation into the skin is very small, but in any case R/NH$_2$-MCM-41 showed the greatest accumulation among studied samples, the cumulative amount of R retained in the skin being 4.61 $\pm$ 0.87, 5.23 $\pm$ 1.10 and 7.52 $\pm$ 1.40 μg cm^{-2} for R, R/MCM-41 and R/NH$_2$-MCM-41, respectively (Fig. 8). Thus, it could be stated that complex-containing hydroalcoholic solution reduced the permeation of R in the receiving phase and provided higher retention in the skin for efficient action. Probably, the presence of ethanol could increase the permeation rate of R, by acting as enhancer and thus by reducing the barrier of the cutis.

To overcome the known side effects of ethanol and to get closer to real conditions, in the present investigation an O/W emulsion was prepared as a topical system for R/silica complexes. Interestingly, after 24 h in this medium the permeation through the skin was negligible for all tested R samples, while the skin retention of R was observed maximum, as in the hydroalcoholic mixture, with R/NH$_2$-MCM-

41 (7.77 μg cm^{-2} ± 1.43), followed by R/MCM-41 (4.54 μg cm^{-2} ± 1.96) and R (1.78 μg cm^{-2} ± 0.87) (Fig. 8). The aforementioned data suggest that the developed R/NH$_2$-MCM-41 may enhance R uptake in the skin, which is necessary for the effective prevention of oxidative skin damage. Thus NH$_2$-MCM-41 can serve as a better topical delivery of this flavonoid.

3.2.3. Antiradical and metal chelating activities

The antioxidant activity of free or immobilized R was firstly determined based on the ability of the flavonoid to act as a radical scavenger towards the stable free radical DPPH$^•$. The method is based on the reduction of the DPPH$^•$ by the presence of a hydrogen-donating species (R, R/MCM-41 or R/NH$_2$-MCM-41) leading to the formation of the non-radical form. Resulting in a color change from purple to yellow by the reaction, the absorbance was followed at increasing R concentrations and data were converted by the equation in radical scavenging activity percentage (% RSA) as reported in Fig. 9.

The above assay was also detected on the mesoporous silica alone in order to investigate if MCM-41 or NH$_2$-MCM-41 could affect the reaction, confirming that both the matrices did not interfere with the DPPH$^•$ assay (data not shown).

In agreement with the literature report a linear correlation between % RSA and R concentration was observed with all the tested samples (Yang et al., 2001). Interestingly, observing Fig. 9 it can be noted that the % RSA of R/MCM-41 is altogether comparable to that of free R. On the contrary, the % RSA values of R/NH$_2$-MCM-41 were lower than those of free R, especially at the highest concentrations, as if the immobilization of the flavonoid in the functionalized silica matrix could partially reduce its antiradical activity. Results may be explained by the lower accessibility of the antioxidant to the DPPH$^•$ radical in the functionalized matrix, whereas already assessed by FTIR analysis, a marked interaction between R molecules and silica aminopropyl groups occurred. Furthermore, this assay confirmed that overall R structure was preserved in the complexes.

22

Metal-binding capacity was investigated by assessing the ability of the antioxidant to compete with the indicator ferrozine to complex ferrous ions in solution. Fig. 10 shows the percentage of Fe^{2+} chelating activity of free R and the complexes at different concentration levels, whereby chelation capacity increased with concentration for investigated samples. Regardless of levels, R/NH$_2$-MCM-41 bound the largest amount of ferrous ions in the assayed samples. It thus exhibited a maximum Fe^{2+} chelating activity of 85% using the highest concentration. This result is reasonably related to the presence of the several aminopropyl groups in the functionalized matrix that could act as metal chelating agents on their own. In fact, aminopropyl silica alone showed already ferrous chelating activity even if the chelating activity obtained by singularly adding those of free R (20%) with NH$_2$-MCM-41 (26%) at the highest concentration (50 µM) is as half active as that of the correspondent complex (85%). At the same time R and R/MCM-41 exhibited very similar binding capacities.

4. Conclusions

The present study involved the immobilization of R in mesoporous silica matrix (MCM-41) in order to stabilize the flavonoid. Complexes, obtained using bare MCM-41 and aminopropyl-functionalized silica (NH$_2$-MCM-41), were characterized by different techniques in order to evaluate the usefulness of functionalization. The complexes, prepared following the methanol impregnation method, showed an efficient loading using functionalized silica, demonstrating a greater affinity with NH$_2$-MCM-41, in agreement with the higher inclusion of R in the pores observed by gas-volumetric analysis. Infrared spectroscopy showed the formation of hydrogen bonded adducts in both matrices, irrespective of surface functionalization, but in the case of functionalized silica the spectroscopic study suggests that the aminopropyl groups play an important role in the interaction with the quercetin aglycone, while on bare silica the interaction takes place through the rutinoside disaccharide.

It is noteworthy that when exposed to UV irradiation mesoporous silica significantly improved R

stability over time indicating a certain capacity in preserving the efficacy against skin damage. In particular, the protection appears to be correlated both with the presence of aminopropyl groups and with the nature of dispersion medium. *Ex vivo* experiments demonstrated that, when complexed with NH$_2$-MCM-41, R established a stronger interaction with the porcine skin allowing a greater accumulation and a reduced permeation. The antioxidant activity of R, analyzed through antiradical activity toward DPPH$^\bullet$ and ferrous ions chelating activity demonstrated that the complexation did not affect R structure, as suggested by infrared analysis.

This study confirmed that R immobilization in MCM-41 and mostly in the aminopropyl functionalized one offers a valid approach to optimize flavonoid physico-chemical properties, to improve the photostability and to increase the skin accumulation. Considering the positive findings of the present research, this mesoporous matrix may be reasonably proposed as an innovative carrier for topical delivery.

References

Ambrogi, V., Perioli, L., Pagano, C., Latterini, L., Marmottini, F., Ricci, M., Rossi C. 2012. MCM-41 for furosemide dissolution improvement. Microporous. Mesoporous. Mater. 147, 343-349.

Ambrogi, V., Zatterini, L., Marmottini, F., Pagano, C., Ricci, M., 2013. Mesoporous silicate MCM-41 as a particulate carrier for octyl methoxycinnamate: Sunscreen release and photostability. J. Pharm. Sci. 102, 1468-1475.

Ambrogio, M.W., Thomas, C.R., Zhao, Y.-L., Zink, J.I., Stoddart, J.F., 2011. Mechanized silica nanoparticles: a new frontier in theranostic nanomedicine. Acc. Chem. Res. 44, 903-913.

Andersson, J., Rosenholm, J., Areva, S., Linden, M., 2004. Influences of material characteristics on ibuprofen drug loading and release profiles from ordered micro- and mesoporous silica matrices. Chem. Mater. 16, 4160-4167.

Beck, J.S., Vartuli, J.C., Roth, W.J., Leonowicz, M.E., Kresge, C.T., Schmitt, K.D., Chu, C.T.W., Olson, D.H., W., S.E., 1992. A new family of mesoporous molecular sieves prepared with liquid crystal templates. J. Am. Chem. Soc. 114, 10834-10843.

Berlier, G., Gastaldi, L., Ugazio, E., Miletto, I., Iliade, P., Sapino, S., 2013. Stabilization of quercetin flavonoid in MCM-41 mesoporous silica: positive effect of surface functionalization. J. Colloid Interface Sci. 393, 109-118.

Braschi, I., Gatti, G., Bisio, C., Berlier, G., Sacchetto, V., Cossi, M., Marchese, L., 2012. The role of silanols in the interactions between methyl *tert*-butyl ether and high-silica faujasite Y: an infrared spectroscopy and computational model study. J. Phys. Chem. C 116, 6943-6952.

Cauda, V., Muehlstein, L., Onida, B., Bein, T., 2009. Tuning drug uptake and release rates through different morphologies and pore diameters of confined mesoporous silica. Microporous Mesoporous Mater. 118, 435-442.

Chen, S.-S., Gong, J., Liu, F.-T, Mohammed, U., 2000. Naturally occurring polyphenolic antioxidants modulate IgE-mediated mast cell activation. Immunology 100, 471-480.

Dall'Acqua, S., Miolo, G., Innocenti, G., Caffieri, S., 2012. The photodegradation of quercetin: relation to oxidation. Molecules 17, 8898-8907.

Di Pasqua, A.J., Sharma, K.K., Shi, Y.-L., Toms, B.B., Ouellette, W., Dabrowiak, J.C., Asefa, T., 2008. Cytotoxicity of mesoporous silica nanomaterials. J. Inorg. Biochem. 102, 1416-1423.

Dinis, T.C.P., Madeira, V.M.C., Almeida, L.A., 1994. Action of phenolic derivatives (acetaminophen,

salicylate, and 5-aminosalicylate) as inhibitors of membrane lipid peroxidation and peroxyl radical scavengers. Arch. Biochem. Biophys. 315, 161-169.

Ferris, D.P., Lu, J., Gothard, C., Yanes, R., Thomas, C.R., Olsen, J.-C., Stoddart, J.F., Tamanoi, F., Zink, J.I., 2011. Synthesis of biomolecule-modified mesoporous silica nanoparticles for targeted hydrophobic drug delivery to cancer cells. Small 7, 1816-1826.

Ferris, D.P., Zhao, Y.-L., Khashab, N.M., Khatib, H.A., Stoddart, J.F., Zink, J.I., 2009. Light-operated mechanized nanoparticles. J. Am. Chem. Soc. 131, 1686-1688.

Fontecave, T., Sanchez, C., Azais, T., Boissiere, C., 2012. Chemical modification as a versatile tool for tuning stability of silica based mesoporous carriers in biologically relevant conditions. Chem. Mater. 24, 4326-4336.

Garcia, A., Colilla, M., Izquierdo-Barba, I., Vallet-Regí, M., 2009. Incorporation of phosphorus into mesostructured silicas: a novel approach to reduce the SiO_2 leaching in water. Chem. Mater. 21, 4135-4145.

Gastaldi, L., Ugazio, E., Sapino, S., Iliade, P., Miletto, I., Berlier, G., 2012. Mesoporous silica as a carrier for topical application: the Trolox case study. Phys. Chem. Chem. Phys. 14, 11318-11326.

Graefe, E., Wittig, J., Mueller, S., Riethling, A., Uehleke, B., Drewelow, B., Pforte, H., Jacobasch, G., Derendorf, H., Veit, M., 2001. Pharmacokinetics and bioavailability of quercetin glycosides in humans. J. Clin. Pharmacol., 41, 492-499.

Gulcin, I., 2006. Antioxidant and antiradical activities of L-Carnitine. Life Sci. 78, 803-811.

Huang, X., Zhuang, J., Teng, X., Li, L., Chen, D., Yan, X., Tang, F., 2010. The promotion of human malignant melanoma growth by mesoporous silica nanoparticles through decreased reactive oxygen species. Biomaterials 31, 6142-6153.

Izquierdo-Barba, I., Sanchez-Salcedo, S., Colilla, M., Feito, M.J, Ramirez-Santillan, C., Portoles, M.T., Vallet-Regí, M., 2011. Inhibition of bacterial adhesion on biocompatible zwitterionic SBA-15

mesoporous materials. Acta Biomater. 7, 2977-2985.

Karthick, M., Prince, P.S.M., 2006. Preventive effect of rutin, a bioflavonoid, on lipid peroxides and antioxidants in isoproterenol-induced myocardial infarction in rats. J. Pharm. Pharmacol. 58, 701-707.

Li, Z., Barnes, J.C., Bosoy, A., Stoddart, J.F., Zink, J.I., 2012. Mesoporous silica nanoparticles in biomedical applications. Chem. Soc. Rev. 41, 2590-2605.

Lin, Y.-S., Abadeer, N., Haynes, C.L., 2011. Stability of small mesoporous silica nanoparticles in biological media. Chem. Commun. 47, 532-534.

Liong, M., France, B., Bradley, K.A., Zink, J.I., 2009. Antimicrobial activity of silver nanocrystals encapsulated in mesoporous silica nanoparticles. Adv. Mater. 21, 1684-1689.

Lu, J., Li, Z., Zink, J.I., Tamanoi, F., 2012. In vivo tumor suppression efficacy of mesoporous silica nanoparticles-based drug-delivery system: enhanced efficacy by folate modification. Nanomedicine 8, 212-220.

Lu, J., Liong, M., Li, Z., Zink, J.I., Tamanoi, F., 2010. Biocompatibility, biodistribution, and drug-delivery efficiency of mesoporous silica nanoparticles for cancer therapy in animals. Small 6, 1794-1805.

Mamaeva, V., Rosenholm, J.M., Bate-Eya, L.T., Bergman, L., Peuhu, E., Duchanoy, A., Fortelius, L.E., Landor, S., Toivola, D.M., Linden, M., Sahlgren, C., 2011. Mesoporous silica nanoparticles as drug delivery systems for targeted inhibition of notch signaling in cancer. Mol. Ther. 19, 1538-1546.

Manzano, M., Colilla, M., Vallet-Regí, M., 2009. Drug delivery from ordered mesoporous matrices. Expert Opin. Drug Deliv. 6, 1383-1400.

Mauludin, R., Müller, R.H., Keck, C.M., 2009. Kinetic solubility and dissolution velocity of rutin nanocrystals. Eur. J. Pharm. Sci. 36, 502-510.

Meng, H., Xue, M., Xia, T., Ji, Z., Tarn, D.Y., Zink, J.I., Nel, A.E., 2011a. Use of size and a copolymer design feature to improve the biodistribution and the enhanced permeability and retention effect of

doxorubicin-loaded mesoporous silica nanoparticles in a murine xenograft tumor model. ACS Nano 5, 4131-4144.

Meng, H., Xue, M., Zink, J.I., Nel, A.E., 2012. Development of pharmaceutically adapted mesoporous silica nanoparticles platform. J. Phys. Chem. Lett. 3, 358-359.

Meng, H., Yang, S., Li, Z., Xia, T., Chen, J., Ji, Z., Zhang, H., Wang, X., Lin, S., Huang, C., Zhou, Z.H., Zink, J.I., Nel, A.E., 2011b. Aspect ratio determines the quantity of mesoporous silica nanoparticle uptake by a small GTPase-dependent macropinocytosis mechanism. ACS Nano 5, 4434-4447.

Middleton, E., Kandaswami, C., Theoharides, T., 2000. The effects of plant flavonoids on mammalian cells: implications for inflammation, heart disease, and cancer. Pharm. Rev. 52, 673-751.

Mortera, R., Fiorilli, S., Garrone, E., Verne, E., Onida, B., 2010. Pores occlusion in MCM-41 spheres immersed in SBF and the effect on ibuprofen delivery kinetics: a quantitative model. Chem. Eng. J. 156, 184-192.

Parida, K.M., Rath, D., 2009. Amine functionalized MCM-41: an active and reusable catalyst for Knoevenagel condensation reaction. J. Mol. Catal. A -Chem. 310, 93-100.

Rabiskova, M., Bautzova, T., Gajdziok, J., Dvorackova, K., Lamprecht, A., Pellequer, Y., Spilkova, J., 2012. Coated chitosan pellets containing rutin intended for the treatment of inflammatory bowel disease: in vitro characteristics and in vivo evaluation. Int. J. Pharm. 422, 151-159.

Rosenholm, J.M., Linden, M., 2008. Towards establishing structure-activity relationships for mesoporous silica in drug delivery applications. J. Controlled Release 128, 157-164.

Rosenholm, J.M., Mamaeva, V., Sahlgren, C., Linden, M., 2012. Nanoparticles in targeted cancer therapy: mesoporous silica nanoparticles entering preclinical development stage. Nanomedicine 7, 111-120.

Rosenholm, J.M., Peuhu, E., Eriksson, J.E., Sahlgren, C., Linden, M., 2009. Targeted intracellular

delivery of hydrophobic agents using mesoporous hybrid silica nanoparticles as carrier systems. Nano Lett. 9, 3308-3311.

Scalia, M., 2009. Incorporation of quercetin in lipid microparticles: effect on photo- and chemical-stability. J. Pharm. Biomed. Anal. 49, 90-94.

Socrates, G., 2004. Infrared and Raman characteristic group frequencies: tables and charts, third ed. John Wiley & Sons Ltd, Chichester, UK.

Tao, Z., Morrow, M.P., Asefa, T., Sharma, K.K., Duncan, C., Anan, A., Penefsky, H.S., Goodisman, J., Souid, A.-K., 2008. Mesoporous silica nanoparticles inhibit cellular respiration. Nano Lett. 8, 1517-1526.

Tosoni, S., Civalleri, B., Pascale, F., Ugliengo, P., 2008. Hydroxylated crystalline edingtonite silica faces as models for the amorphous silica surface. J. Phys.: Conf. Ser. 117, 012026.

Trewyn, B., Nieweg, J., Zhao, Y., Lin, V., 2008. Biocompatible mesoporous silica nanoparticles with different morphologies for animal cell membrane penetration. Chem. Eng. J. 137, 23-29.

Vallet-Regí, M., Balas, F., Arcos, D., 2007. Mesoporous materials for drug delivery. Angew. Chem. Int. Ed. Engl. 46, 7548-7558.

Vallet-Regí, M., Ramila, A., del Real, R.P., Pérez-Pariente, J., 2001. A new property of MCM-41: drug delivery system. Chem. Mater. 13, 308-311.

Vivero-Escoto, J., Slowing, I., Trewyn, B., Lin, V., 2010. Mesoporous silica nanoparticles for intracellular controlled drug delivery. Small 18, 1952-1967.

Wang, S., 2009. Ordered mesoporous materials for drug delivery. Microporous Mesoporous Mater. 117, 1-9.

Yang, B., Kotani, A., Arai, K., Kusu, F., 2001. Estimation of the antioxidant activities of flavonoids from their oxidation potentials. Anal. Sci. 17, 599-604.

Figure captions

Scheme 1. Structure of rutin molecule.

Fig. 1. XRD patterns of MCM-41 (full black), NH_2-MCM-41 (dotted), R/MCM-41 (full grey) and R/NH_2-MCM-41 (dashed).

Fig. 2. Thermogravimetric analysis of: a) MCM-41 (full black); b) NH_2-MCM-41 (dotted); c) R/MCM-41 (full grey); d) R/NH_2-MCM-41 (dashed).

Fig. 3. Nitrogen adsorption/desorption isotherms measured on: a) MCM-41; b) R/MCM-41; c) NH_2-MCM-41; d) R/NH_2-MCM-41. Curves were vertically shifted for easier comparison.

Fig. 4. Pore volume distribution profiles of a) MCM-41 (□); b) R/MCM-41 (○); c) NH_2-MCM-41 (△) and d) R/NH_2-MCM-41 (✕).

Fig. 5. FTIR spectra in the high and low frequency regions (top and bottom, respectively) of MCM-41 (full black); R/MCM-41 (full grey); free R (short dotted).

Fig. 6. FTIR spectra in the high and low frequency regions (top and bottom, respectively) of NH_2-MCM-41 (full black); R/NH_2-MCM-41 (full grey); free R (short dotted).

Fig. 7. Diffusion profiles of R (◆), R/MCM-41 (■) and R/NH$_2$-MCM-41 (▲) from the hydroalcoholic mixture through the dialysis membrane. Each bar represents the mean ± SD obtained in three independent experiments.

Fig. 8. Skin permeation and uptake profiles of tested formulations after 24 h *ex vivo* study. Each bar represents the mean ± SD obtained in three independent experiments.

Fig. 9. Antiradical activity (expressed as % RSA) of free R, R/MCM-41 and R/NH$_2$-MCM-41 towards DPPH$^•$. Each bar represents the mean ± SD obtained in three independent experiments.

Fig. 10. Chelating activity percentage of free R, silica matrices and complexes. Each bar represents the mean ± SD obtained in three independent experiments.
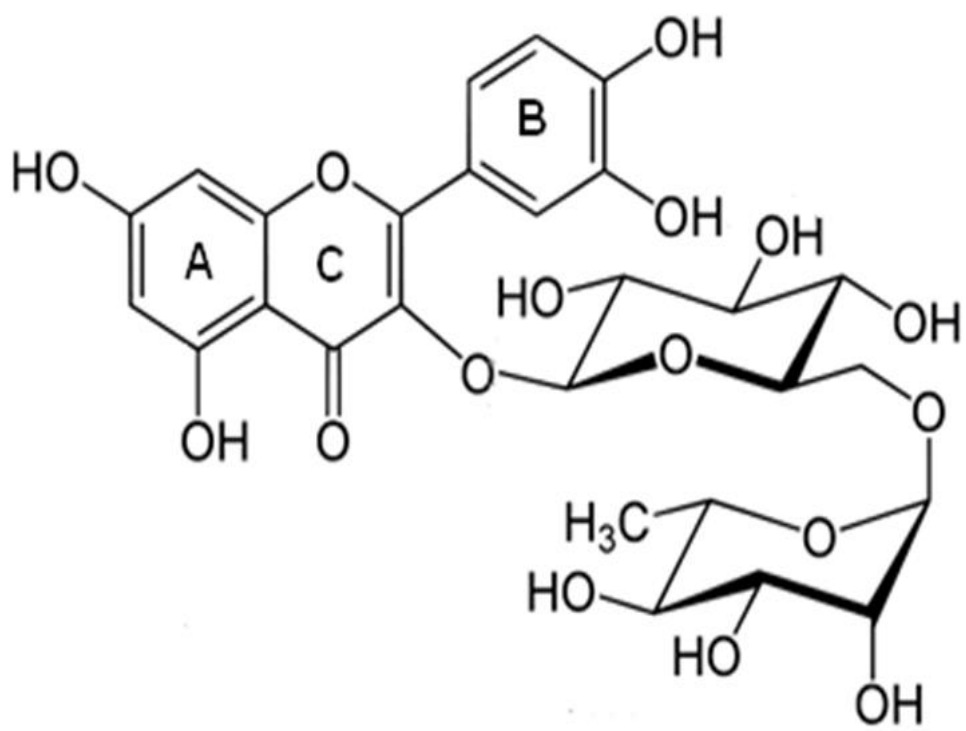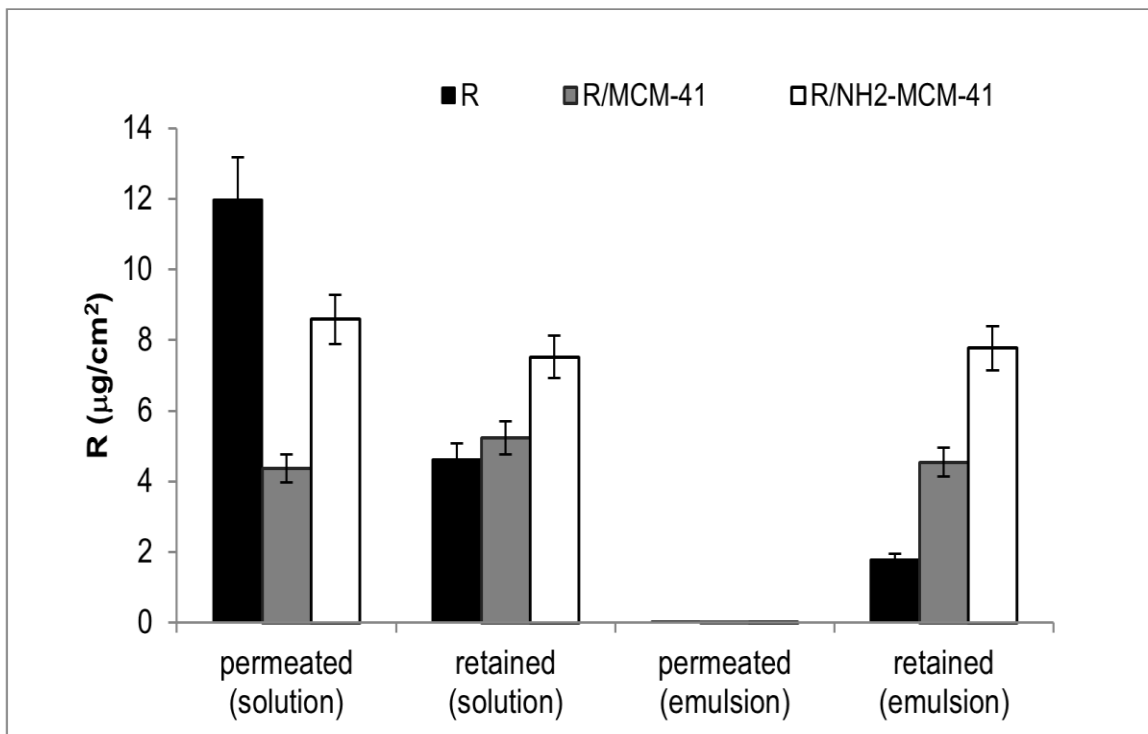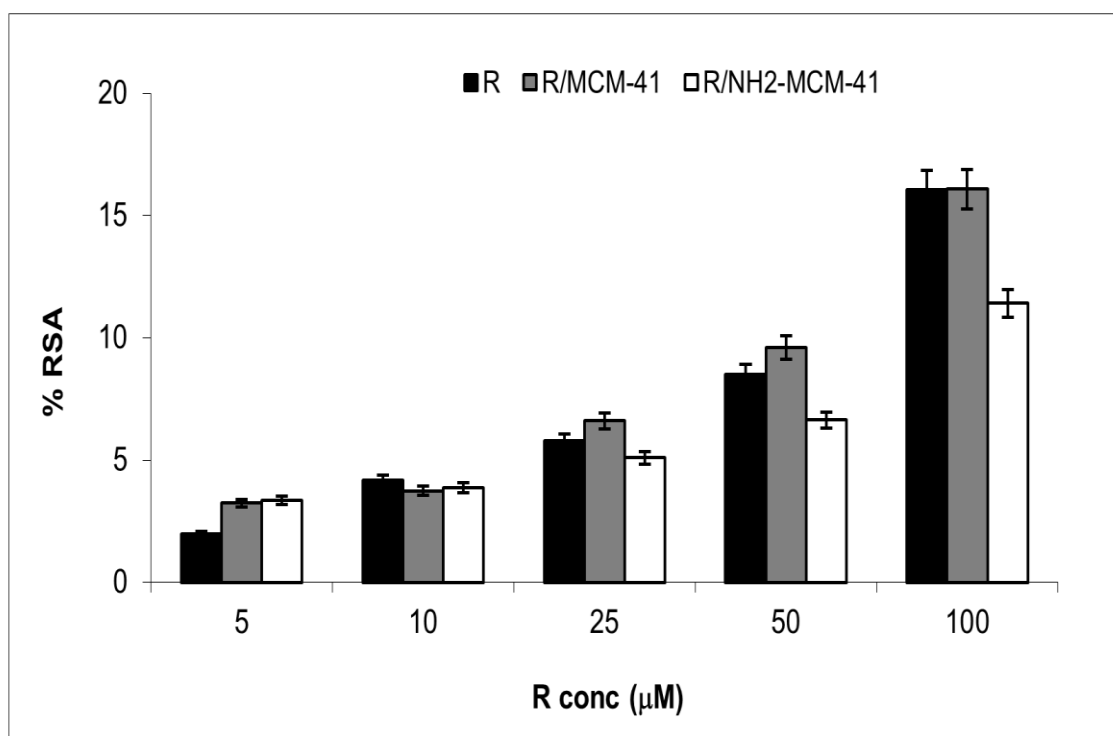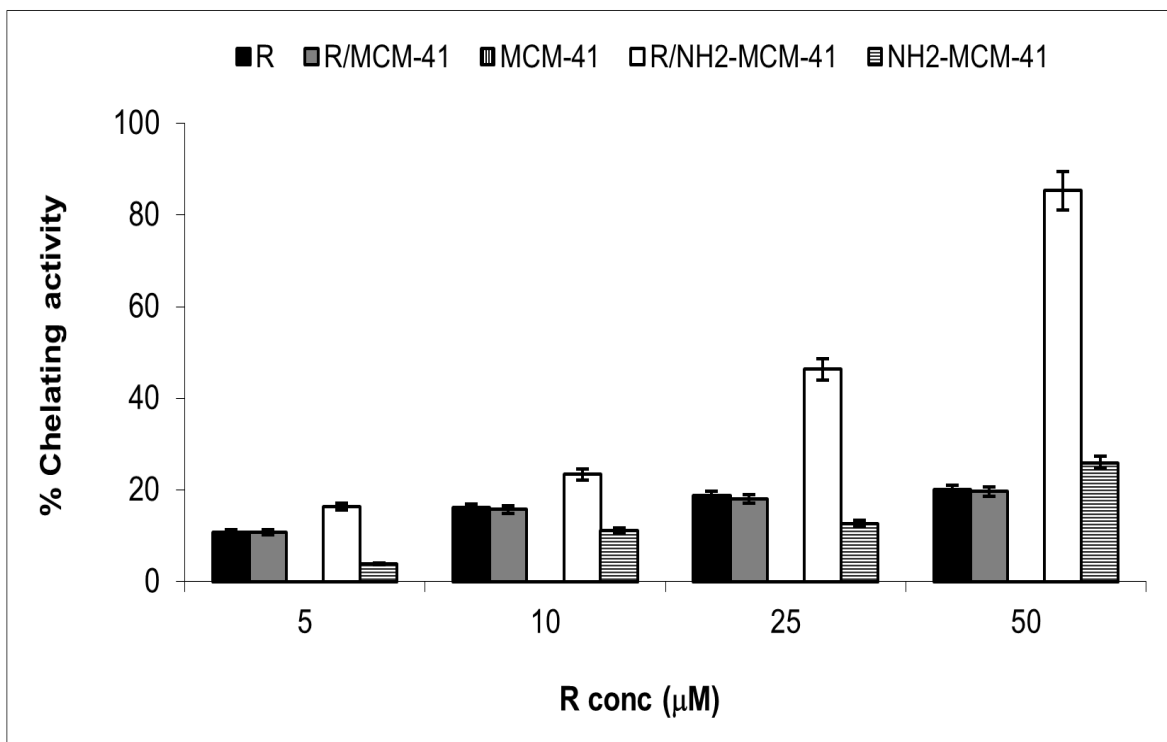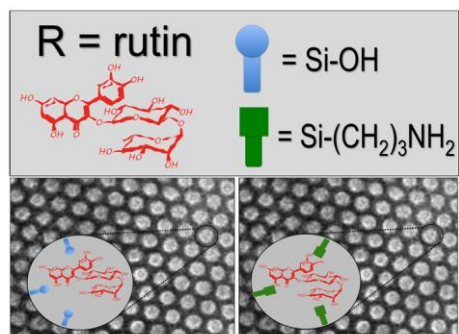
Scheme 1
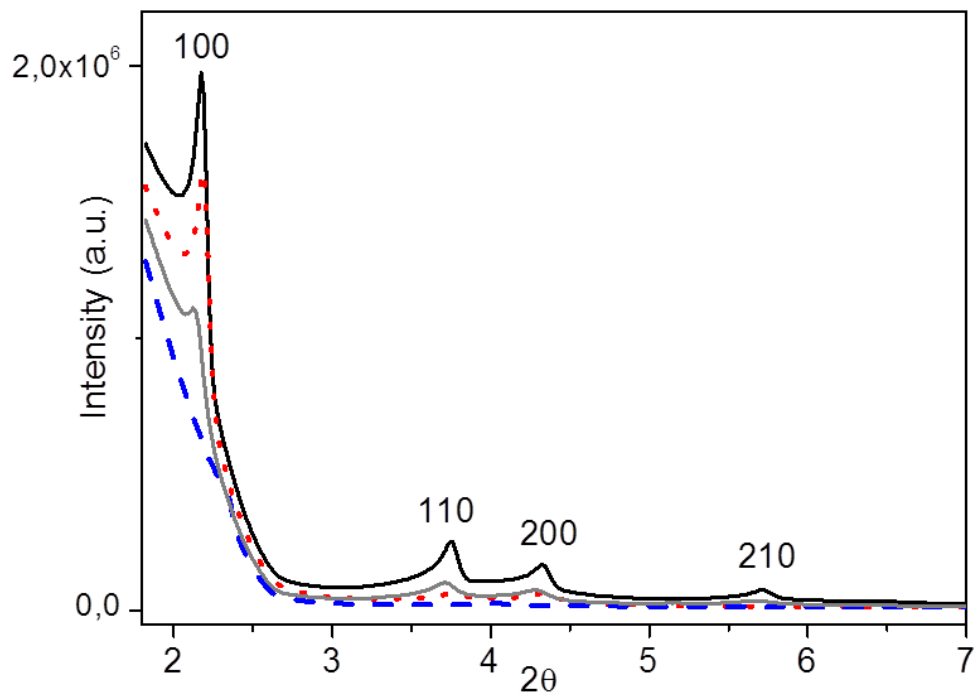
Figure 1
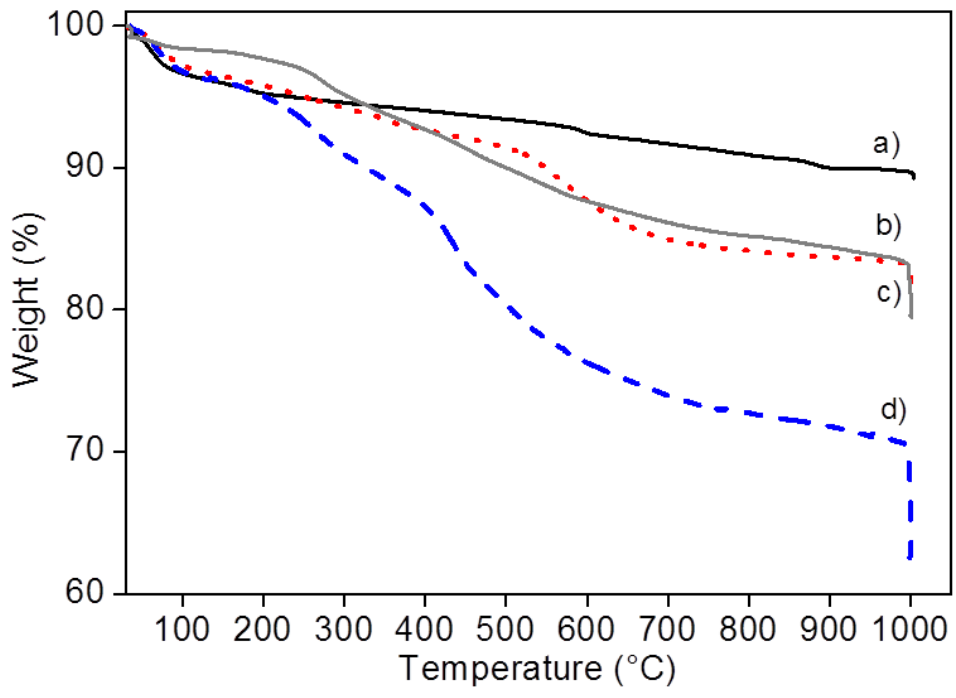
Figure 2
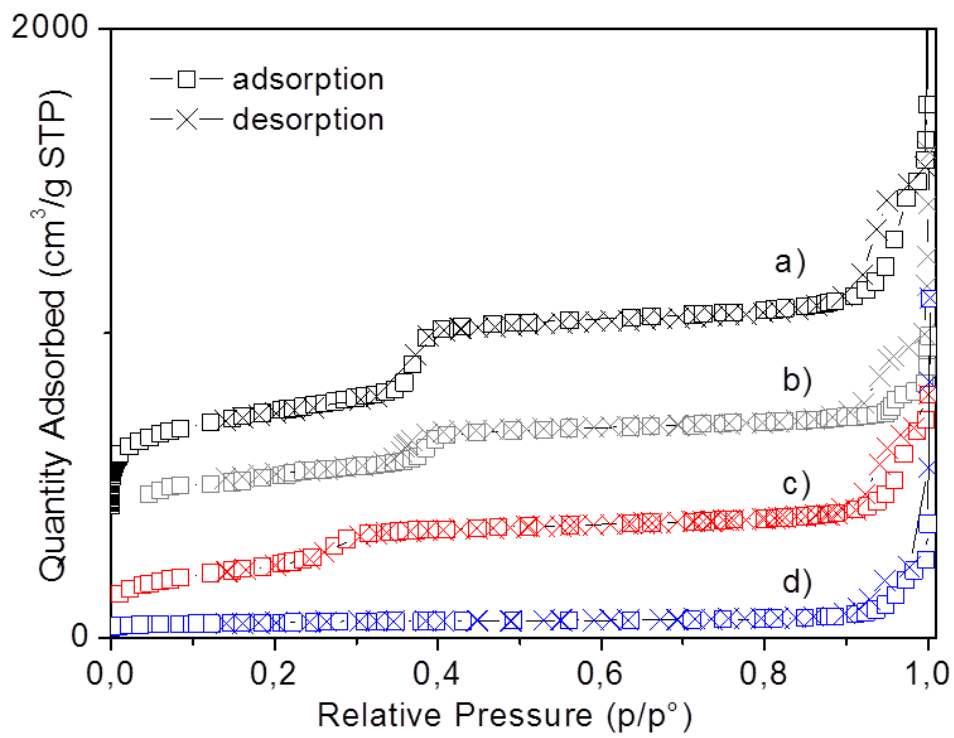
Figure 3
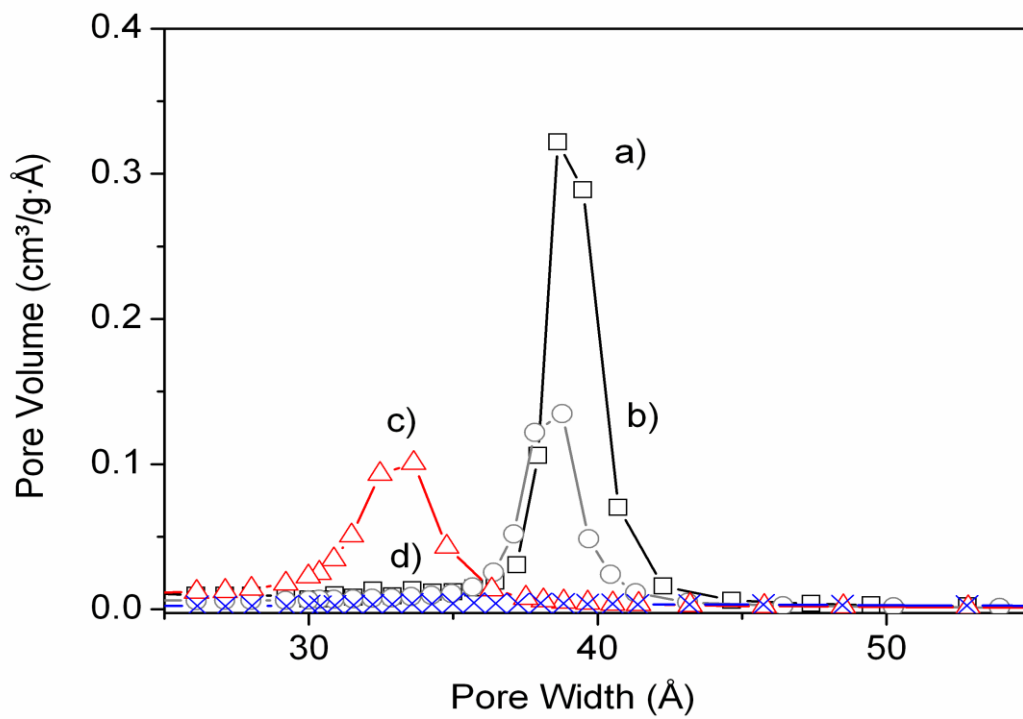
Figure 4
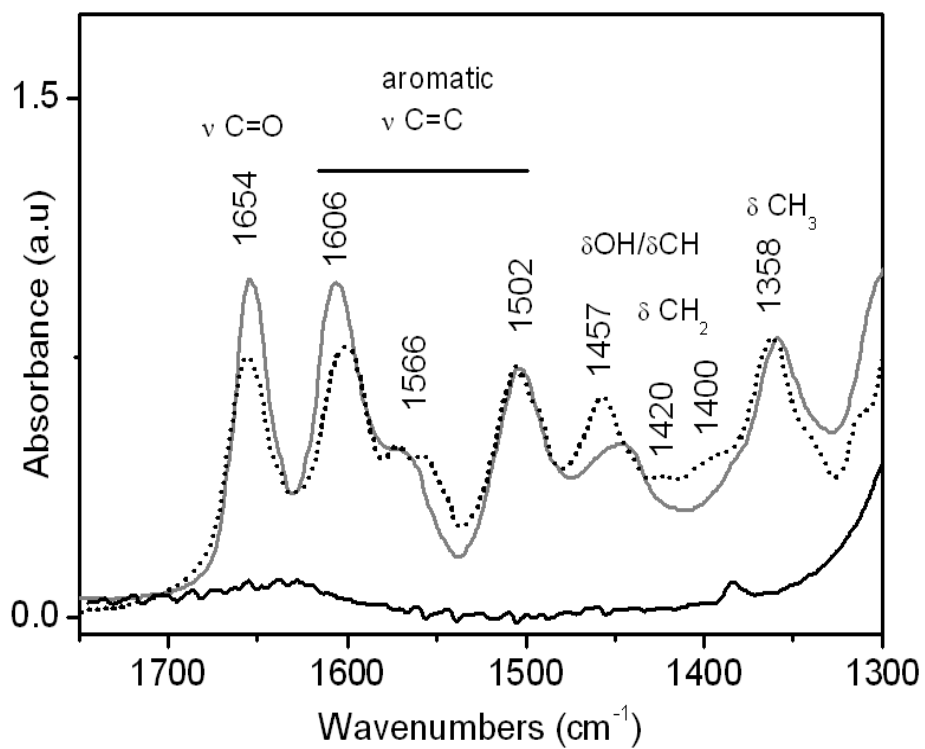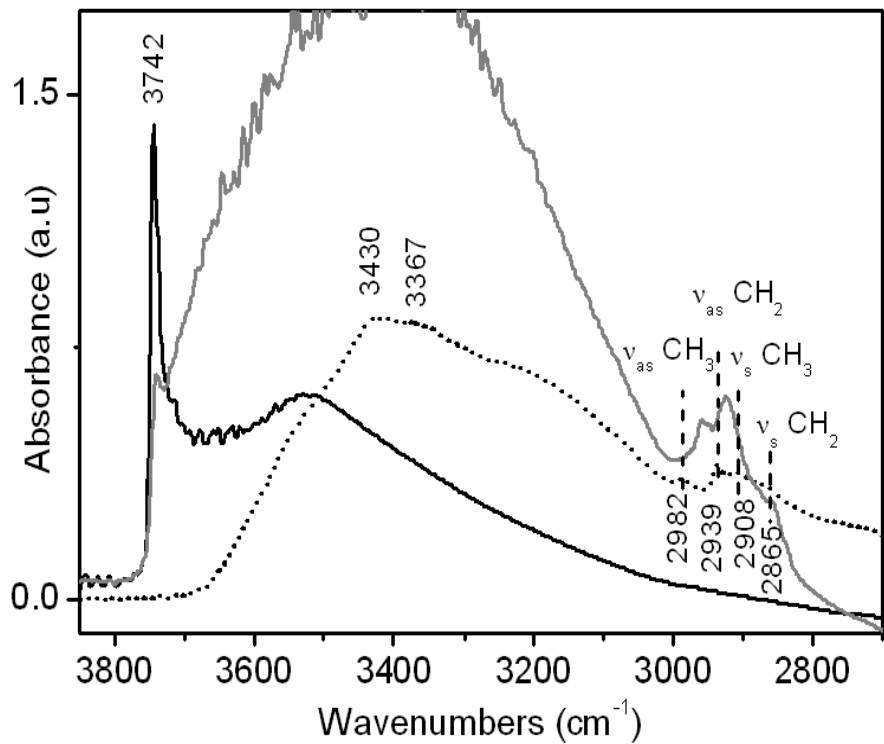
Figure 5
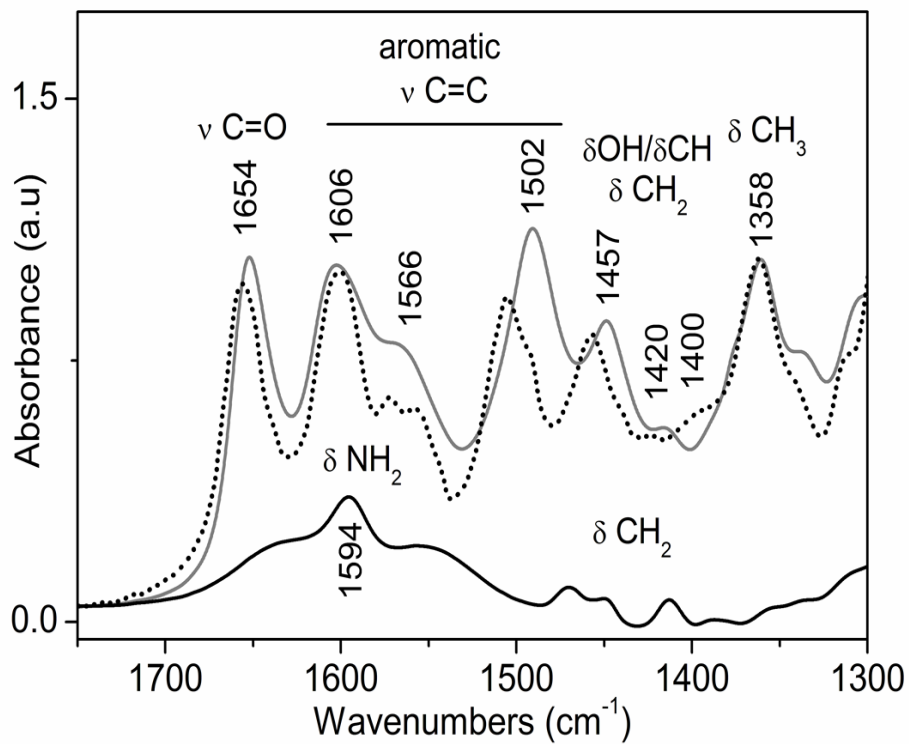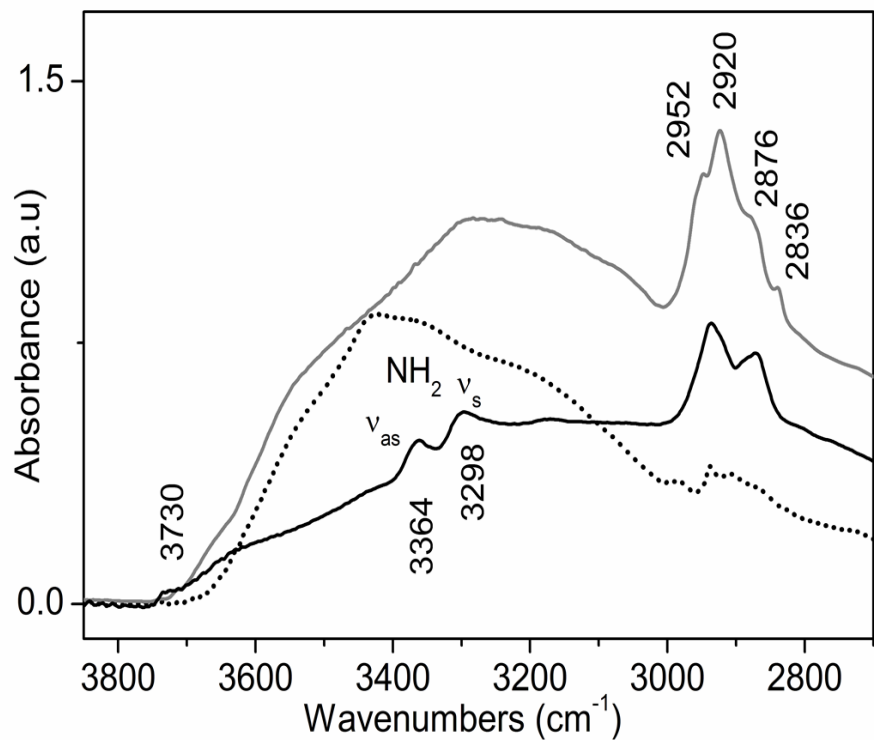
Figure 6
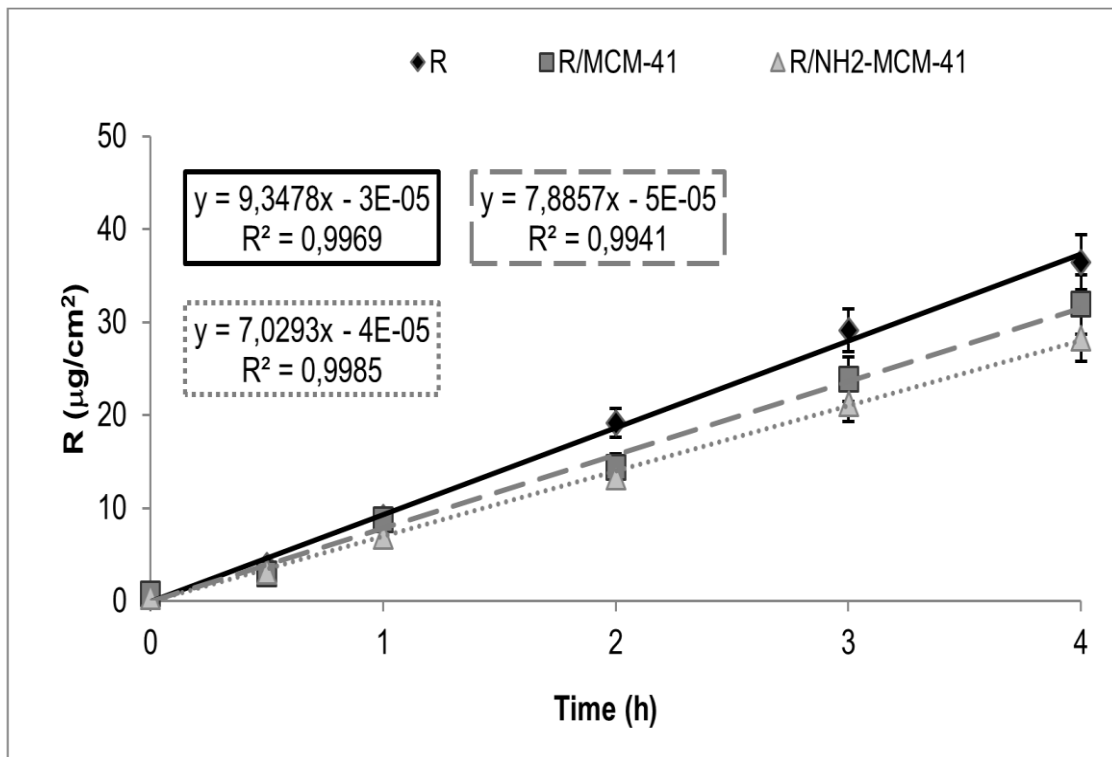
Figure 7

Figure 8

Figure 9

Figure 10

Graphical abstract